# Journal of Materials Chemistry A

Accepted Manuscript


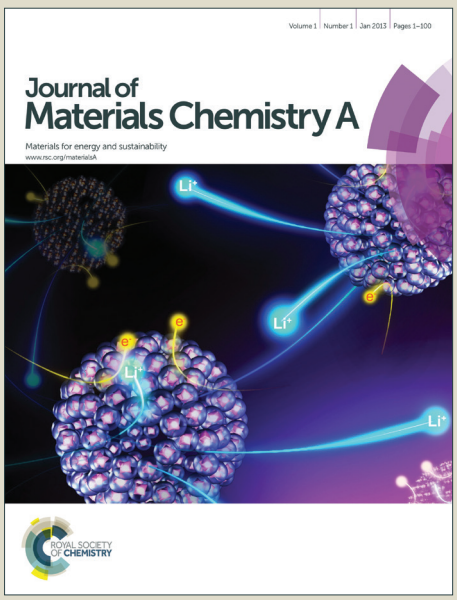





ROYAL SOCIETY OF CHEMISTRY

www.rsc.org/materialsA

**Graphic abstract**

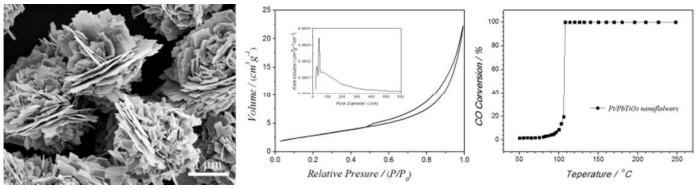


3D flower-like $PbTiO_3$ nanostructures self-assembled with (101) nanosheets have been realized via a facile hydrothermal rout and show excellent ability to enhance the catalytic activity of Pt as supports for the oxidation of CO because of the well mesoporous structures and high specific surface area.

Cite this: DOI: 10.1039/c0xx00000x

www.rsc.org/xxxxxx

ARTICLE TYPE

# Self-assembled 3D flower-like Perovskite $PbTiO_3$ nanostructures and their application in the catalytic oxidation of CO

**Gang Xu,* Huiwen Bai, Xiaoqiang Huang, Wanbo He, Lingling Li, Ge Shen, Gaorong Han**

***Received (in XXX, XXX) Xth XXXXXXXXX 20XX, Accepted Xth XXXXXXXXX 20XX***
**DOI: 10.1039/b000000x**

3D flower-like $PbTiO_3$ nanostructures self-assembled with (101) nanosheets have been realized by hydrothermal treatment the mixture of the lead and titanium hydroxides under the effect of the high KOH concentration. The layered $K_2Ti_6O_{13}$ formed in situ under the effect of the high KOH concentration plays an important role in the crystallization of the primary $PbTiO_3$ nanosheets and the further self-assembly of the 3D flower-like perovskite $PbTiO_3$ nanostructures. The self-assembled 3D flower-like perovskite $PbTiO_3$ nanostrucutres express well mesoporous structures and high specific surface area. In consequence, the 3D flower-like perovskite $PbTiO_3$ nanostructures as supports show excellent ability to enhance the catalytic activity of Pt. Over the Pt/$PbTiO_3$ nanoflowers, the CO instantaneously converses to $CO_2$ completely at a very low temperature of ca. 107 $^oC$, facilitating the catalytic purification of the automotive exhaust produced in the cold start period.

## Introduction

Automotive exhaust, mainly composed of carbon monoxide (CO), nitrogen oxides ($NO_x$), unburned hydrocarbons ($CH_x$), and sulfur oxides ($SO_x$), is one of the main generators of air pollutants.[1-3] This problem is expected to control by catalytic purification, in which CO is oxidized to carbon dioxide ($CO_2$). Up to now, the automotive exhaust purified emission indeed has been realized under the effect of the noble metal three-way catalysts. However, the catalytic purification of the automotive exhaust produced in the cold start period is still difficult because of the catalytic converter's inability at low temperatures.[4]

Perovskite-based materials have been investigated, since 1970s,[5] as promising automotive exhaust catalysts to replace the existing noble metal-based catalysts due to their surface redox properties, high bulk oxygen mobility and good thermal stability.[6-8] Because the perovskite-based materials are generally less active for hydrocarbon oxidation than noble metal catalysts,[6,9,10] a lot of investigations are performed on the perovskite-based materials as supports to enhance the catalytic activity of the noble metal catalysts.[10-12] For example, impregnating Pd over perovskite $LaMnO_3$-based materials produces active catalysts for methane combustion[10,11] and Pt-supported on the perovskite $SrTiO_3$ nanocuoid effectively promotes the propane oxidation.[12] Lead titanate, $PbTiO_3$, is a typical perovskite oxide. Below about 490 $^oC$, $PbTiO_3$ has a distorted perovskite structures and consequently displays spontaneous polarization. In our recent experiment, it has been demonstrated that when the Pt nanoparticles are supported over the $PbTiO_3$ nanoplates, the catalytic activity is significantly improved, making the catalytic oxidation of CO completely achieved at a very low temperature of about 100 $^oC$.[13] Whereas the catalytic oxidation of the carbon monoxide occurs on the surface of the catalysts,[14,15] it is essential to prepare the $PbTiO_3$ catalyst carriers of high specific surface area for the instantaneous oxidation of the carbon monoxide involved in the automotive exhaust especially in the cold-start period.

Three-dimensional (3D) nanostructures have attracted intensive attentions because of their unique properties and potentials applications. [16-27] Generally the 3D nanostructures are self-assembled with primary building blocks, such as nanocrystallites, nanorods and nanosheets, in a spontaneous process. As the primary building blocks are nanosheets, the 3D nanostructures traditionally express high specific surface area and well mesoporous structures. Due to the high adsorption ability, the 3D flower-like iron oxide nanostructures self-assembled with nanosheets show an excellent ability to remove heavy metal ions and other pollutants in water treatment.[19] Since the ultrathin primary nanosheets facilitate the fast Li ion diffusion and the effective accommodation of the large volumetric change occurred during the discharge and charge processes, the 3D hierarchical flower-like ZnO, TiO2 nanoflowers as anode in Li-ion battery exhibit significant improvements in reversible capacities and cycle performance.[21,26, 27] Similarly, because of the high specific surface area and the mesoporous structures, it is expected that the 3D flower-like $PbTiO_3$ nanostructures self-assembled with nanosheets as supports would significantly enhance the instantaneous catalytic oxidation of CO under the effect of the supported Pt catalysts.

However, the synthesis of the perovskite oxide nanosheets is a challenge. Over the past decades, as an important kind of ferroelectric materials, perovskite oxide nanostructures have been attracted considerable attentions.[28] Despite the less anisotropic lattice, a lot of perovskite 1D nanostructures have been realized

by bottom-up chemical routes. Park and his co-workers firstly realize the synthesis of the $BaTiO_3$ and $SrTiO_3$ nanowires by the solution-phase decomposition of the bimetallic alkoxide precursors in the presence of the coordinatin ligands.[29] After a while, a more suitable method was proposed in our previous researching works. The tetragonal perovskite $PbZr_{0.52}Ti_{0.48}O_3$ nanorods and nanowires are hydrothermally synthesized by assisted with the polymer.[30] In virtue of the adsorption of the organic surfactant, Rørvik and his co-workers also realize the hydrothermal synthesis of the $PbTiO_3$ hierarchical nanostructures self-assembled with nanorods. [22,23] As for the perovskite oxide nanosheets, only a few reports are obtained.[31,32] Although the $PbTiO_3$ nanosheets with a size of about 10 nm in thickness have been successfully synthesized via a conventional hydrothermal route in our recent researching work, a lot of $PbTiO_3$ particles also form at the same time.[33]

Hydrothermal technique is an aqueous-based precipitation route. Since the crystal nucleation and growth can be easily controlled over by tuning the hydrothermal reaction conditions, such as hydrothermal treatment temperature, during time, starting precursors, mineralizer, feedstocks, and modifiers, hydrothermal route is widely used to synthesize inorganic functional nanostructures with various morphologies. Herein, 3D flower-like $PbTiO_3$ nanostructures self-assembled with (101) nanosheets have been realized by a traditional and facile hydrothermal route. The layered $K_2Ti_6O_{13}$ nanofibers formed in advance under the effect of the high KOH concentration during the hydrothermal treatment play a critical role. Due to the substitution of $Pb^{2+}$ ions for the $K^+$ ions, the TiO6 octahedron lamella exfoliate from the $K_2Ti_6O_{13}$ lattice and transform to lamellar $PbTiO_3$ species by combining the $Pb^{2+}$ ions. Then, these special lamellar $PbTiO_3$ species crystallize to the $PbTiO_3$ nanosheets and the further self-assembled 3D flower-like $PbTiO_3$ nanostructures. Because of the high specific surface area and the mesoporous structures, the 3D flower-like $PbTiO_3$ nanostructures as supports of the noble metal Pt make the catalytic oxidation of CO instantaneously achieved at a very low temperature.

## Experimental procedures

All of the chemicals used in this work, including tetrabutyl titanate $(C_4H_9O)_4Ti$ , lead nitrate $Pb(NO_3)_2$, ethanol, potassium hydroxide (KOH), and ammonia were analytical grade purity and used without further purification. Distilled water was used in the preparation of all aqueous solutions.

The hydrothermal treatment was carried out in a homemade Teflon-lined stainless-steel autoclave. Lead and titanium were introduced into the hydrothermal system in the form of the precipitated lead and titanium hydroxides. When preparing the precipitates of lead and titanium hydroxides, ammonia was used as precipitant. In a typical procedure, $Pb(NO_3)_2$ and $(C_4H_9O)_4Ti$ dissolve in distilled water and absolute ethanol, respectively. The formed ethanol $(C_4H_9O)_4Ti$ solution and aqueous $Pb(NO_3)_2$ solution was added into dilute ammonia solution in turn under the continuous magnetic stirring for precipitating titanium and lead hydroxides. After filtering and washing with distilled water for six times, the obtained precipitate mixture of lead and titanium hydroxides was then dispersed in distilled water with vigorous magnetic stirring, followed by the addition of KOH pellets. After continuous magnetic stirring for 6 h, the suspension was adjusted to 40 mL and poured into a 50 mL stainless-steel Teflon-line autoclave for hydrothermal treatment. In the final feedstock suspension, a titanium concentration of 0.13 $molL^{-1}$, a Pb/Ti molar ratio of 1.4:1, and a KOH concentration of 12 $molL^{-1}$ were created. The hydrothermal treatment was performed by placing the sealed autoclave in an oven and keeping it at 200 $^oC$ for 24 h, and then cooled it to room temperature in air. The products were filtered and washed for several time, first with distilled water and then with absolute ethanol, and finally oven dried in air at 60 $^oC$ for 24 h. In order to understand the formation mechanism of the 3D flower-like $PbTiO_3$ nanostructures, the hydrothermal treatment time was adjusted in the range of 0.5-24 h and the Pb/Ti molar ratio was designated as 1.1:1, 1.2:1, 1.3:1, and 1.4:1, respectively, meanwhile other hydrothermal conditions were riveted.

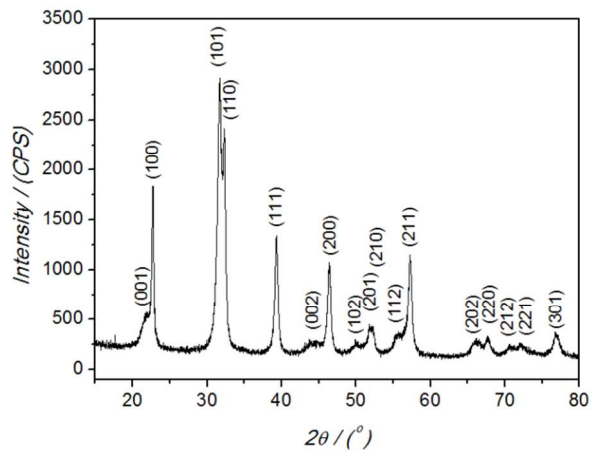


**Fig. 1** XRD pattern of the sample hydrothermally synthesized under the effect of 12 molL-1 KOH at 200 $^oC$ for 24 h

X-ray powder diffraction (XRD) patterns were obtained by Rigaku D/max-RA X-ray diffractometer with high-intensity Cu Ka (λ=1.5418 Å) radiation with a step size of 0.02º. Scanning elelctron microscopy (SEM) measurements and energy dispersive spectroscopy (EDS) were performed using a Hitachi S-4800 microscope (Japan). Transmission electron microscopy (TEM) images were taken with a FEI Tecnai G2 F30 TEM at 160 kV and a high-resolution TEM (HRTEM) images were caught at 200 kV. Nitrogen adsorption-desorption isotherms were measured at 77 K with a Quantachrome Autosorb Automated Gas Sorption System.

In order to evaluated the promotion effect of the 3D flower-like $PbTiO_3$ nanostructures as carrier on the catalytic activity of Pt catalyst, Pt nanoparticles was attached on the surfaces of the 3D flower-like $PbTiO_3$ nanostructures. The synsthesized 3D $PbTiO_3$ flower-like nanostructures were dispersed in distilled water in an unltrasonic bath for 30 min. A 0.05 $molL^{-1}$ aqueous solution of chloroplatinic acid ($H_2PtCl_6{\cdot}6H_2O$) was then added into the above suspension. After continuous ultrasonic stirring for 15 min at room temperature, a 0.2 $molL^{-1}$ NaBH4 solution was introduced dropwise. The 3D flower-like Pt/$PbTiO_3$ nanostructures were obtained after centrifugation and washing with distilled water for six times, and then drying at 60 $^oC$ for 24 h. Measurement of the catalytic activity for the carbon monoxide catalytic oxidation reaction were carried out in a quartz flow tube



 

reactor. 20 mg (40–60 mesh) of a 1 % flower-like Pt/$PbTiO_3$ nanostructure powders was packed in the reactor and pretreated at 250 °C for 2 h under a dry $H_2/N_2$ flow (50 mL/min). After cooling to room temperature, a gas mixture typically containing 0.7 vol % CO and 33.3 vol % ($O_2$+He) was introduced into the reactor at 30 $mLmin^{-1}$ in the temperature range from room temperature to 250 °C. The composition of the reactants and the products was analyzed by a gas chromatograph (GC-14C) equipped with a thermal conductivity detector (TCD) on line.

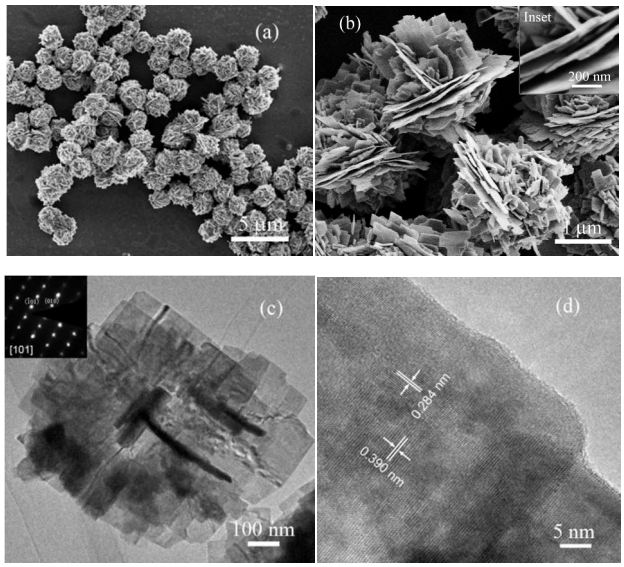


**Fig. 2** (a) and (b) SEM, (c) TEM, and (d) HRTEM images of the hydrothermally synthesized 3D flower-like perovskite $PbTiO_3$ nanostructures. Inset in (b) is the local magnification for determining the thickness of the primary nanosheets

## Results and discussion

Figure 1 shows the XRD pattern of the sample hydrothermally synthesized under the effect of 12 $molL^{-1}$ KOH at 200 °C for 24 h. A simple identification of the XRD pattern demonstrated that the powders are of the pure tetragonal perovskite $PbTiO_3$ with lattice constant of a=3.90 Å and c=4.15 Å, matching well with the reported literature values at the standard card of JCPDS No. 06-0452. The SEM image shown in Figure 2a reveals that the obtained $PbTiO_3$ samples are composed of uniform 3D flower-like nanostructures with an approximate 2-3 μm in diameter. The corresponding EDS spectrum indicates that the 3D flower-like $PbTiO_3$ nanostructures consist of Pb, Ti an O with ratio of about 1:1:3, agreeing well with the nominal chemical composition of $PbTiO_3$ perovskite. The detail morphology of the flower-like nanostructure shown in Figure 2b as a magnified SEM image illustrates that the entire 3D flower-like $PbTiO_3$ nanostrucuture is self-assembled by nanosheets with smooth surface. These primary block nanosheets are ca. 10-20 nm in thickness and ca. 2-3 μm in the max width. Moreover, in one 3D flower-like $PbTiO_3$ nanostructure some nanosheets overlap parallel and connect with others perpendicularly. The 3D flower-like $PbTiO_3$ nanostructures were further characterized by TEM and HRTEM in turn. Representative TEM and HRTEM images of one single 3D flower-like $PbTiO_3$ nanostructures are presented in Figure 2c and d, respectively. Due to the upright nanosheets, a few dark lines are observed over the flat parallel nanosheets. The SAED pattern as inset shown in Figure 2c is caught from the corresponding flat parallel nanosheets. Because the SAED pattern can be indexed as [101], it is relational to argue that the primary blocks, $PbTiO_3$ nanosheets, are dominated with (101) facets. Therefore, two sets of lattice fringes with intervals of 0.390 and 0.284 nm, which agree well with the spacing of (100) and (101) planes, respectively, are observed in the HRTEM image shown in Figure 2d.

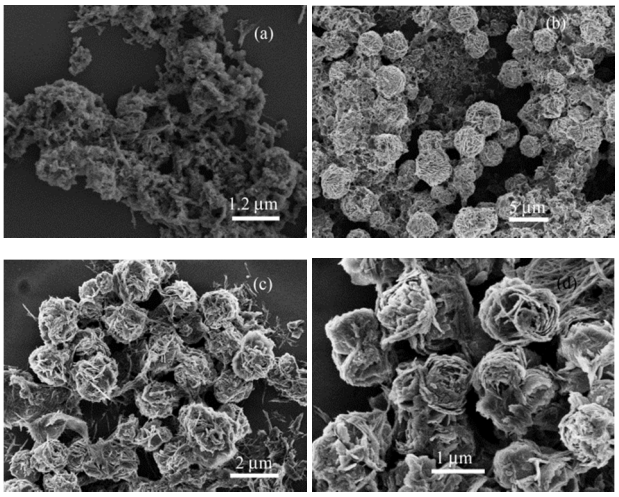


**Fig. 3** SEM images of the samples obtained after hydrothermal treatment for different time, (a) 0.5, (b) 4, (c) 8, and (d) 16 h

In order to understand the formation mechanism of the 3D flower-like $PbTiO_3$ nanostructures, a set of time-dependent hydrothermal experiments were carried out. Fig. S1 (See supporting informations) shows the XRD patterns of the samples obtained after hydrothermal treatment the mixture precursorsfor different time. At the initial stage, the hydrothermal treatment time less than 0.5 h, only two diffraction peaks of the layered $K_2Ti_6O_{13}$ overlap the broad XRD pattern, implying the obtained samples are composed of layered $K_2Ti_6O_{13}$ and amorphous phases. With the hydrothermal treatment time prolongation to over 4 h, all the diffraction peaks of the obtained samples can be indexed to the tetragonal perovskite lattice of $PbTiO_3$ (JCPDS No. 06-0452), indicating the all obtained samples are of perovskite $PbTiO_3$ crystals. Moreover, with the hydrothermal treatment further prolongation, the diffraction peaks gradually become sharp and intense, pointing out the synthesized $PbTiO_3$ crystals grow larger and of improved crystallinity. Figure 3 presents the SEM images of the samples obtained after hydrothermal treatment the mixture precursors for different time. A few nanofibers are observed reflecting the formation of the layered $K_2Ti_6O_{13}$ [34] but for the amorphous floccule in the samples obtained at the initial stage of the hydrothermal reaction (Figure 3a). With the formation of the perovskite $PbTiO_3$, a lot of 3D flower-like $PbTiO_3$ nanostructures appear in the samples obtained by hydrothermal treatment the mixture precursors for 4 h over the few nanofibers and the few amorphous floccules (Figure 3b). As the hydrothermal treatment time prolongs to 8 h, corresponding to the enhancement of the XRD diffraction peaks of the perovskite $PbTiO_3$ phase the 3D flower-like nanostructures predominate the obtained samples (Figure 3c). When the hydrothermal treatment

time increases to 16 h, the nanofibers and amorphous phases are hardly found and only 3D flower-like $PbTiO_3$ nanostructures are observed from the synthesized samples (Figure 3d). Nonetheless, it should be noticed that at the moment the 3D flower-like $PbTiO_3$ nanostructures are self-assembled by roll nanosheers, very different from the one obtained at the hydrothermal treatment for 24 h (see Figure 2).

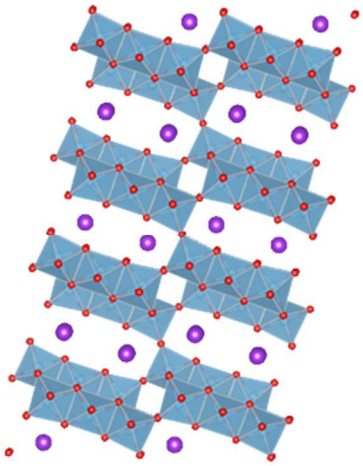

**Fig. 4** Structural model of the layered $K_2Ti_6O_{13}$ compound

It has been demonstrated that with titanium hydroxide precipitates as titanium sources, the tetragonal perovskite $PbTiO_3$ sample hydrothermal synthesized at low KOH concentration are of cubic particles,[35] well reflecting the intrinsic symmetry of the tetragonal perovskite lattice. In the present experiment, due to the formation of the layered $K_2Ti_6O_{13}$ nanofibers in advance under the effect of the high KOH concentration the subsequent $PbTiO_3$ crystallizes to nanosheets and self-assembles to 3D flower-like nanostructures instead of the cubic particles. Therefore, it is believed that the formed layered $K_2Ti_6O_{13}$ nanofibers in advance play an important role in the synthesis of the 3D flower-like $PbTiO_3$ nanostructures.

Figure 4 shows the structural model of the layered $K_2Ti_6O_{13}$ compound, in which the $TiO_6$ octahedrons construct the 2D layers by sharing edges and corners and the 2D $TiO_6$ octahedron layers link together by connecting the corners of the opposing octahedrons. $K^+$ ions insert in the tunnels formed between the 2D $TiO_6$ octahedron layers. Many experiments have demonstrated that the layered $K_2Ti_6O_{13}$ nanofibers are easily synthesized by hydrothermal treatment the titanium oxide or hydroxide at high KOH concentrations.[35-39] Moreover, because the $K^+$ ions inserted in the tunnels between the 2D $TiO_6$ octahedron layers are easily exchanged, the perovskite $BaTiO_3$ and $PbTiO_3$ nanorods are successfully prepared by employing the layered potassium titanate nanofibers as template, respectively.[40-42] In the present experiment, because the concentration of the used minerallizer KOH is very high, a lot of $K_2Ti_6O1_3$ nanofibers form in advance at the initial hydrothermal treatment stage (Fig. S1 and Figure 3a). With the hydrothermal treatment prolongation, $Pb^{2+}$ ions gradually substitute for the inserted $K^+$ ions in the layered $K_2Ti_6O_{13}$ lattice by undergoing the $Pb^{2+}$ ion diffusion and the dehydration of the lead hydroxide under the hydrothermal conditions. As the substitution of the $Pb^{2+}$ ions for the inserted $K^+$ ions in the layered $K_2Ti_6O_{13}$ lattice accumulates to a certain extent, the layered titanate lattice becomes unstable and some $TiO_6$ octahedron lamella exfoliate from the layered titanate structure by breaking the connecting corners of the opposing octahedrons, which belong to the opposite $TiO_6$ octahedron layers. The exfoliated $TiO_6$ octahedron lamella as template further react with the dehydrated $Pb^{2+}$ ions to form lead titanate lamellar species, in which the edge-shared $TiO_6$ octahedron lamella transform to corner-shared $TiO_6$ lamella for pursuing more stability. Subsequently, the lead titanate lamellar species crystallize to tetragonal perovskite $PbTiO_3$ nanosheets. Whereas the primary nanosheets for the self-assembled 3D flower-like $PbTiO_3$ nanostructures are dominated with (101) facets, with the basis of the perovskite structure lattice it can be suggested that the lamellar $PbTiO_3$ species are of zigzag corner-shared $TiO_6$ octahedron lamellar frameworks. Because the limitation along the normal direction is less than that along the flat of the nanosheets, the lamellar $PbTiO_3$ species with zigzag corner-shared $TiO_6$ octahedron frameworks crystallize to $PbTiO_3$ nanosheets with dominant (101) and (011) facets rather than (110) facets.

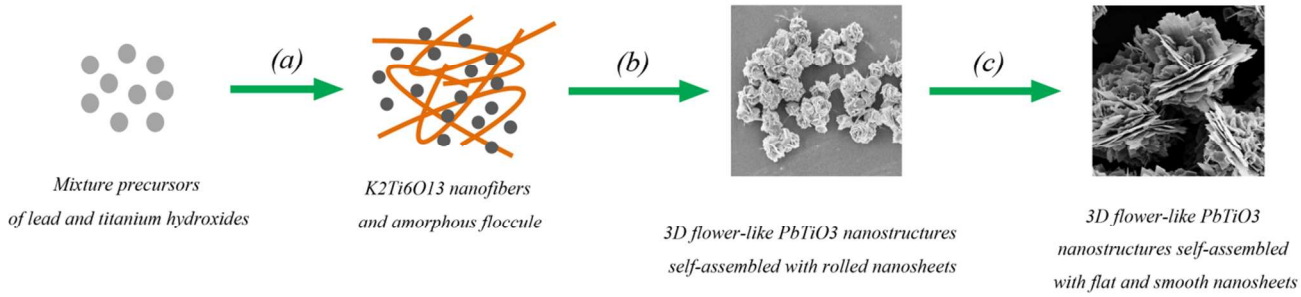


**Fig. 5** Schematic illustration of the hydrothermal synthesis process of the 3D flower-like pervoskite $PbTiO_3$ nanostructures self-assembled with nanoshets. (a) In the initial stage, due to the effect of the high KOH concentration the titanium hydroxides dehydrate and condense to a few layered $K_2Ti_6O_{13}$ nanofibers by reacting with the KOH. (b) With the hydrothermal treatment prolongation, the lead hydroxides also dehydrate and the Pb2+ ions substitute for the K+ ions inserted in the layered $K_2Ti_6O_{13}$ crystal structure, resulting in the formation of the $PbTiO_3$ nanosheets. Because the formed $PbTiO_3$ nanosheets are very thin and of intensive stress, the $PbTiO_3$ nanosheets self-assemble to 3D flower-like $PbTiO_3$ nanostructures by overlapping and rolling. (c) After an Ostwald ripening process, the primary $PbTiO_3$ nanosheets become flat and smooth. Accordingly, the 3D flower-like $PbTiO_3$ nanostructures are of smooth $PbTiO_3$ nanosheets by overlapping and setting upright with others

In the initial stage, the formed $PbTiO_3$ nanosheets are very thin and a lot of defects are involved in it. Thus, it is reasonable to

think that there are intensive stresses existed in the very thin $PbTiO_3$ nanosheets. This strong stresses facilitate the $PbTiO_3$ nanosheets to roll. On the other hand, in order to minimize the system energy the formed $PbTiO_3$ nanosheets are apt to overlap parallel. The cooperation of the two effects results in the formed $PbTiO_3$ nanosheets self-assemble to 3D flower-like $PbTiO_3$ nanostructures by overlapping and rolling (Figure 3b-d). With the hydrothermal reaction proceeding, more amounts of 3D flower-like $PbTiO_3$ nanostructures form by expending the amorphous floccules and the formed layered $K_2Ti_6O_{13}$ nanofibers in advance. As the hydrothermal treatment prolongs to a moderate time, about 16 h, the amorphous precursors and the formed layered $K_2Ti_6O_{13}$ nanofibers in advance is exhausted and the synthesized samples entirely consist of 3D flower-like $PbTiO_3$ nanostructures self-assembled by the parallel and rolled nanosheets (Figure 3d). Whereas at this time the primary nanosheets are very thin and a lot of stresses are involved in it, an Ostwald ripening process would be brought about with the hydrothermal treatment prolongation, in which the primary nanosheets grow thick and smooth. Moreover, because the two planes of (011) and (101) together belong to the group of {101} in the tetragonal perovskite $PbTiO_3$ structure and are perpendicular each other, after undergoing the Ostwald ripening process in one 3D flower-like $PbTiO_3$ nanostructure some nanosheets overlap parallel and set upright with others (Figure 2a and b). To summarize the discussion above, a scheme is simply depicted in Figure 5 for illustrating the formation process of the 3D flower-like perovskite $PbTiO_3$ nanostructures self-assembled with nanosheets

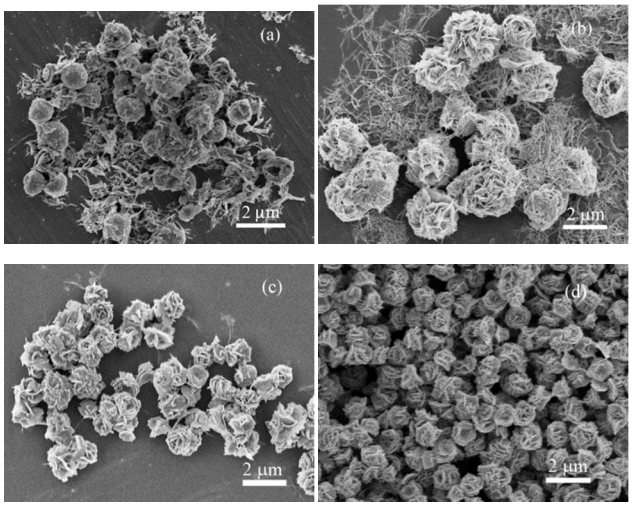


**Fig. 6** SEM images of the samples obtained by hydrothermal treatment the mixture precursors with different Pb/Ti molar ratio of (a) 1:1, (b) 1.2:1, (c) 1.3:1 and (d) 1.4:1 at 200oC for 16 h

The investigation on the effect of the Pb/Ti molar ratio on the synthesis of the 3D flower-like $PbTiO_3$ nanostructures also confirms the correction of the proposed formation mechanism above. Figure 6 shows the SEM images of the samples synthesized with different Pb/Ti molar ratio at 200 $^oC$ hydrothermal treatment for 16 h. According to the chemical reaction theory, as more amount of Pb precursors are added in the hydrothermal system, the reaction for the formation of the $PbTiO_3$ nanosheets by the $Pb^{2+}$ ion substitution for the $K^+$ ion in the layered $K_2Ti_6O_{13}$ is enhanced. Thus, after hydrothermal treatment for 16 h the synthesized samples with Pb/Ti molar ratio higher than 1.3:1 entirely consist of flower-like $PbTiO_3$ nanostructures (Figure 6c and 6d), whereas a lot of $K_2Ti_6O_{13}$ nanofibres are obviously observed but for the flower-like $PbTiO_3$ nanostructures in the samples synthesized with Pb/Ti molar ration less than 1.2:1 (Figure 6a and 6b).

Figure 7 shows the nitrogen adsorption-desorption isotherm and Barrett-Joyner-Halenda (BJH) pore size distribution curve (inset) of the 3D flower-like $PbTiO_3$ nanostructures obtained by hydrothermal treatment the mixture precursors at 200 $^oC$ for 24 h. The isotherm shows a type IV pattern with hysteresis loop, indicating the well developed mesopores in the self-assembled 3D flower-like $PbTiO_3$ nanostructures. The BET specific area, pore volume and mean pore diameter are about 10.46 $m^2/g$, 0.033 $cm^3/g$ and 112 nm, respectively. Many researching works have demonstrated that perovskite-based materials as supports can significantly enhance the catalytic activity of the noble metal catalyst.[10-13] Whereas the catalytic oxidation of CO occurs on the surfaces of the catalysts, it is expected that the 3D flower-like $PbTiO_3$ nanostructures would benefit the instantaneous CO oxidation as catalyst Pt carriers because of the large specific area.

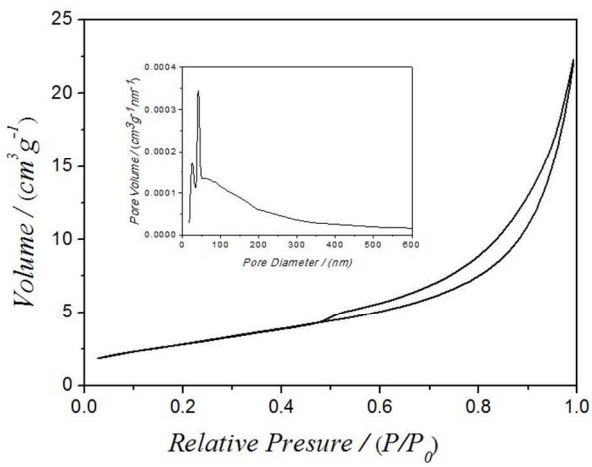


**Fig. 7** Nitrogen adsorption-desorption isotherms and pore size distribution curve (inset) of the hydrothermally synthesized 3D flower-like perovskite $PbTiO_3$ nanostructures

The catalytic effectiveness over the Pt-attached flower-like $PbTiO_3$ nanostructures (hereafter denoted as Pt/$PbTiO_3$ nanoflowers) for the catalytic oxidation of CO was shown in Figure 8. As a control, the catalytic oxidation of CO under the effect of Pt/$PbTiO_3$ nanoplates [13] was also presented in Figure 8. The STEM image and the EDX element maps demonstrated that the Pt nanoparticles are well attached and dispersed on the surfaces of the primary $PbTiO_3$ nanosheets, which are the primary blocks for the self-assembly of the $PbTiO_3$ nanoflowers. (See Fig. S2 in the supporting inforamtions). Due to the effect of the spontaneous polarization of the tetragonal perovskite $PbTiO_3$ crystals,[13] both Pt/$PbTiO_3$ nanoflowers and Pt/$PbTiO_3$ nanoplates display excellent catalytic performance for the oxidation of CO to $CO_2$. The lowest complete conversion temperature for the both catalysts is obviously lower than that Pt supported on other oxides with non-ferrolectricity, such as Pt/CeO (about 144 $^oC$).[43] Nonetheless, between the two lowest complete conversion temperatures there is a narrow difference of about 7 $^oC$. The

lowest complete conversion temperature for the Pt/$PbTiO_3$ nanoflowers (about 107 °C) is slightly higher than that for the Pt/$PbTiO_3$ nanoplates (about 100 °C). Otherwise, the onset temperature of the oxidation of CO for the Pt/$PbTiO_3$ nanoflowers (about 75 °C) is also higher than that for the Pt/PbTiO3 nanoplates (about 60 °C). The difference between the two onset temperatures (about 15 °C) is broader than that between the corresponding two lowest complete conversion temperatures (about 7 °C). The catalytic oxidation of CO under the effect of Pt/$PbTiO_3$ flowers undergoes a dramatic enhancement in a narrow temperature range from 103 °C to 107 °C. Below 103 °C, the conversion ratio of CO is very low. At 103 °C the conversion ratio of CO to $CO_2$ is still less than 14%. As over 103 °C, however, the oxidation of CO dramatically enhances and achieves completely at 107 °C.

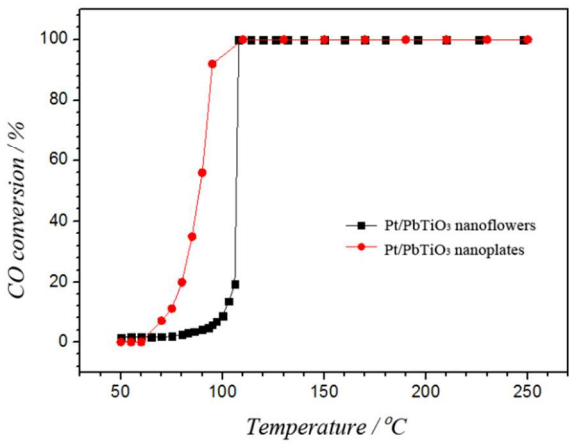


**Fig. 8** Percentage conversion versus temperature curves for the catalytic oxidation of CO over Pt/$PbTiO_3$ nanoflowers and Pt/$PbTiO_3$ nanoplates

It is well known that ferrolelectricity represents a cooperative phenomenon that relies on the interaction of neighbouring permanent electric dipoles in a crystal lattice. There is a size-limit, known as the superparaelectric limit, below which ferroelectricity vanishes. Whereas the thickness of the primary nanosheets for the self-assembly of the $PbTiO_3$ nanoflowers is much thinner than that of the $PbTiO_3$ nanoplates, thus, it is relational to think that the $PbTiO_3$ nanoflowers self-assembled with nanosheets displays weaker spontaneous polarization compared to the $PbTiO_3$ nanoplates. Moreover, it is well known that the spontaneous polarization along [001] direction is the strongest. The primary nanosheets of the self-assembled $PbTiO_3$ nanoflowers are dominated with (101) facets, whereas the $PbTiO_3$ nanoplates are dominated with (001) facets. The difference in the spontaneous polarization between the $PbTiO_3$ nanoflowers and the $PbTiO_3$ nanoplates is further enhanced. In consequence, the Pt/$PbTiO_3$ nanoflowers express smaller catalytic activity than the Pt/$PbTiO_3$ nanoplates. Therefore, both the onset temperature and the lowest conversion temperature of the oxidation of CO over the Pt/$PbTiO_3$ nanoflowers are higher than that over the Pt/$PbTiO_3$ nanoplates (Figure 8). On the other hand, it is generally accepted that the catalytic process is mainly related to the adsorption and desorption of gas molecules on the surfaces of the catalyst. The high specific surface area of the Pt/$PbTiO_3$ nanoflowers results in more unsaturated surface coordination site exposed to the CO gas, bringing about the dramatic enhancement of the oxidation of CO over the Pt/$PbTiO_3$ nanoflowers in a narrow temperature range from 103 °C to 107 °C. Because the onset temperature is mainly determined by the intrinsic spontaneous polarization, the onset temperature over the Pt/$PbTiO_3$ nanoflowers is 15 °C higher than that over the Pt/$PbTiO_3$ nanoplates. However, due to the effect of the high specific surface area the lowest complete conversion temperature over the Pt/$PbTiO_3$ nanoflowers is only slightly 7 °C higher than that over the Pt/$PbTiO_3$ nanoplates

## Conclusion

In summary, 3D flower-like $PbTiO_3$ nanostructures self-assembled with nanosheets have been synthesized by a facile and conventional hydrothermal route with lead and titanium hydroxide as precursors under the effect of high KOH concentrations. The primary nanosheets for the self-assembly of the 3D flower-like $PbTiO_3$ nanostructures are dominated with (101) facets. The 3D flower-like $PbTiO_3$ nanostructures are of well developed mesoporous structures. The BET specific area, pore volume and mean pore diameter are ca. 10.46 $m^2$/g, 0.033 $cm^3$/g and 112 nm, respectively, for the 3D flower-like $PbTiO_3$ nanoshtructures obtained after hydrothermal treatment for 24 h. The high KOH concentration plays an important role in the formation the $PbTiO_3$ nanosheets and the self-assembly of the 3D flower-like $PbTiO_3$ nanostructures. Due to the effect of the high KOH concentration, in the initial stage of the hydrothermal treatment the layered $K_2Ti_6O_{13}$ lamellar crystals form firstly. In the proceeding hydrothermal treatment, the formed layered $K_2Ti_6O_{13}$ lamellar crystals in advance as templates transform to lamellar $PbTiO_3$ species by the diffusion and substitution of the $Pb^{2+}$ ions dehydrated from the lead hydroxide for the $K^+$ ions inserted in the layered lattice of the $K_2Ti_6O_{13}$. The formed lamellar $PbTiO_3$ species further crystallize to tetragonal perovskite $PbTiO_3$ nanosheets with dominant (101) facets. In the initial stage, the crystallized $PbTiO_3$ nanosheets are very thin and immediately self-assemble to 3D flower-like nanostructures by overlapping parallel and curving for stabilization. As the precursors completely transform to 3D flower-like $PbTiO_3$ nanostructures, an Ostwald ripening process occurs, resulting in the primary nanosheets become flat and thick. In addition, due to the high specific surface area and the spontaneous polarization, as supports the 3D flower $PbTiO_3$ nanostructures strongly promote the instantaneous catalytic oxidation of CO under effect of the supported Pt. In a very narrow temperature range, from 103 °C to 107 °C, the conversion ratio of CO to $CO_2$ over the Pt/$PbTiO_3$ nanoflowers instantaneously changes from 14% to 100%. It is believed that the finding in the present experiment proposes a possibility to realize the catalytic purification of the automotive exhaust produced in the cold start period.

## Acknowledgements

The authors wish to thanks the National Natural Science Foundation of China under grant number 61274004 and 51232006, and the Zhejiang Natural Science Foundation, China, under grant number LY12B07007, and Key Science and Technology Innovation Team of Zhejiang Province under grant number 2010R50013.



 

## Notes and references

*State Key Laboratory of Silicon Materials and Department of Materials Science and Engineering, Zhejiang University, Hangzhou 310027, China. Tel: 86-571-87951649; Fax: 86-571-87952341. E-mail: msegxu@zju.edu.cn, hgr@zju.edu.cn.*

† Electronic Supplementary Information (ESI) available: XRD patterns of the samples obtained after hydrothermal treatment for different time and the STEM image, element Pb, Pt, O and Ti EDX map of the Pt/$PbTiO_3$ nanofloweres. See DOI: 10.1039/b000000x/

1 C. Chang, J. Lo, J. Wang, Atmos. Environ. 2001, 35, 6201.
2 Z. D. Ristovski, E. R. Jayaratne, L. Morawska, G. A. Ayoko, M. Lim, Sci. Total Environ. 2005, 345, 93.
3 M. Tanaka, Y. Tsujimoto, T. Miyazaki, M. Warashina, S. Wakamatsu, Chemosphere, 2001, 3, 185.
4 R. Heck, R. Farrauto, Appl. Catal. A 2001, 221, 443.
5 W. F. Libby, Science, 1971, 171, 499.
6 M. Alifanti, J. Kirchnerova, B. Delmon, D. Klvana, Appl. Catal. A, 2004, 262, 167.
7 L. Simonot, F. Garin, G. Maire, Appl. Catal. B, 1997, 11, 167.
8 A. Boreave, H. Tan, V. Roche, P. Vernoux, J.-P. Deloume, Solid State Ionics, 2008, 179, 1071.
9 A. Musialik-Piotrowska, H. Landmesser, Catal. Today, 2008, 137, 357.
10 A. Civera, G. Negro, S. Specchia, G. Saracco, V. Specchia, Catal. Today, 2005, 100, 275.
11 L. Giebeler, D. Kiessling, G. Wendt, Chem. Eng. Technol. 2007, 30, 889.
12 J. A. Enterkin, W. Setthapum, J. W. Elam, S. T. Christensen, F. S. Rabuffetti, L. D. Marks, P. C. Stair, K. R. Poeppelmeier, C. L. Marshall, ACS Catal. 2011, 1, 629-635.
13 C. Y. Chao, Z. H. Ren, Y. H. Zhu, Z. Xiao, Z. Y. Liu, G. Xu, J. Q. Mai, X. Li, G. Shen, G. R. Han, Angew, Chem. Int. Ed. 2012, 51, 9281-9287.
14 S. Nagarajan, K. Thirunavukkarasu, C. S. Gopinath, J. Phys. Chem. C, 2009, 113, 7385-7397.
15 F. G. Wang, K. F. Zhao, H. J. Zhang, Y. M Dong, T. Wang, D. N. He, Chem. Engineer J. 2014, 242, 10-18.
16 Z. Tang, S. Shen, J. Zhuang, X. Wang, Angew. Chem. Int. Ed. 2010, 49, 4603.
17 S. Ding, D. Zhang, J. S. Chen, X. W. Lou, Nanoscale, 2012, 4, 95.
18 P. P. Wang, H. Y. Sun, Y. J. Ji, W. H. Li, X. Wang, Adv. Mater. 2014, 26, 964-969.
19 L. S. Zhong, J. S. Hu, H. P. Liang, A. M. Cao, W. G. Song, L. J. Wan, Adv. Mater. 2006, 18, 2426-2431.
20 Y. F. Zhang, G. Xu, X. Wei, Z. H. Ren, Y. Liu, G. Shen, G. R. Han, CrystEngComm, 2012, 14, 3702.
21 F. Li, L. L. Yang, G. Xu, X. Q. Huang, X. Yang, X. Wei, Z. H. Ren, G. Shen, G. R. Han, J. Alloys and Compounds, 2013, 577, 663-668.
22 G. Wang, R. Sæterli, P. M. Rørvik, A. T. J. van Helvoort, R. Holmestad, T. Grande, and M. A. Einarsrud, Chem. Mater. 2007, 19, 2213.
23 P. M. Rørvik, T. Grande, M. A. Einarsrud, Crystal Growth & Design, 2009, 9, 1979-1984.
24 R. F. Service, Science, 2005, 309, 95.
25 L. Y. Mao, Y. R. Wang, Y. J. Zhong, J. Q. Ning, Y. Hu, J. Mater. Chem. A, 2013, 1, 8101.
26 X. J. Lü, F. Q. Huang, X. L. Mou, Y. M. Wang, F. F. Xu, Adv. Mater. 2010, 22, 3718-3722.
27 S. J. Ding, Y. M. Wang, Z. L. Hong, X. J. Lü, D. Y. Wan, F. Q. Huang, Chem. Eur. J. 2011, 17, 11535-11541.
28 P. M. Rørvik, T. Grande, M. A. Einarsrud, Adv. Mater. 2011, 23, 4007-4034.
29 J. J. Urban, W. S. Yun, Q. Gu, H. K. Park, J. Am. Chem. Soc. 2002, 124, 1186.
30 G. Xu, Z. H. Ren, P. Y. Du, G. Shen, G. R. Han, Adv. Mater. 2005, 17, 907-910.
31 X. Yang, G. Xu, Z. H. Ren, X. Wei, C. Y. Chao, S. Y. Gong, G. Shen, G. R. Han, CrystEngComm, 2014, 16, 4176.
32 G. Xu, X. Q. Huang, Y. F. Zhang, S. Q. Deng, X. Wei, G. Shen, G. R. Han, CrystEngComm, 2013, 15, 7206.
33 G. Xu, X. Q. Huang, V. Krstic, S. Q. Chen, X. Yang, C. Y. Chao, G. Shen, G. R. Han, CrystEngComm, 2014, 16, 4373.
34 Du, G. H. ; Chen, Q.; Han, P. D.;etc. Potassium titanate nanowires: Structure, growth, and optical properties, Phys. Rev. B, 2003, 67, 035323.
35 Z. Y. Liu, Z. H. Ren, X. Wei, Z. Xiao, X. H. Hou, G. Shen, G. Xu, G. R. Han, J. Am. Ceram. Soc. 2010, 93, 3610-3613.
36 Wang, R. H. ; Chen, Q. ; Wang, B. L.;etc. Applied Phys. Lett. 2005, 86, 133101.
37 R. Menzel, A. M. Peiró, J. R. Durrant, M. S. P. Shaffer, Chem. Mater. 2006, 18, 6059-6068.
38 K. Kiatkittipong, C. H. Ye, J. Scott, R. Amal, Crystal Growth & Design 2010, 10, 3618-3625.
39 T. Zhang, Q. Chen, L. M. Peng, Adv. Funct. Mater. 2008, 18, 3018-3025.
40 S. O. Kang, H. S. Jang, K. B. Kim, B. H. Park, M. J. Jung, Y. I. Kim, Mater. Res. Bull. 2008, 43, 996-1003.
41 Z. Y. Cai, X. R. Xing, R. B. Yu, X. Y. Sun, G. R. Liu, Inorg. Chem. 2007, 46, 7423-7427.
42 P. M. Rørvik, T. Lyngdal, R. Sæterli, A. T. J. van Helvoort, R. Holmestad, T. Grande, M. A. Einarsrud, Inorg. Chem. 2008, 47, 3173-3181.
43 H. P. Zhou, H. S. Wu, J. Shen, A. X. Yin, L. D. Sun, C. H. Yan, J. Am. Chem. 2010, 132, 4998-4999.